International Journal of Engineering, Mathematical and Physical Sciences
ISSN: 2517-9934
Vol:7, No:1, 2013

A Computational Fluid Dynamic Model of Human Sniffing

M.V. Shyla, K.B. Naidu

***Abstract*—**The objective of this paper is to develop a computational model of human nasal cavity from computed tomography (CT) scans using MIMICS software. Computational fluid dynamic techniques were employed to understand nasal airflow. Gambit and Fluent software was used to perform CFD simulation. Velocity profiles, iteration plots, pressure distribution, streamline and pathline patterns for steady, laminar airflow inside the human nasal cavity of healthy and also infected persons are presented in detail. The implications for olfaction are visualized. Results are validated with the available numerical and experimental data. The graphs reveal that airflow varies with different anatomical nasal structures and only fraction of the inspired air reaches the olfactory region. The Deviations in the results suggest that the treatment of infected volunteers will improve the olfactory function.

***Keywords*—**CFD techniques, Finite Volume Method, Fluid dynamic sniffing, Human nasal cavity.

I. Introduction

SNIFFING is sampling the surrounding fluid by the sensory detection(olfaction) of an odor or scent in the environment [1]. The developments in medical imaging together with techniques in computational fluid dynamics have led to new possibilities for anatomically realistic numerical simulations of nasal airflow. Elad et al. [2], Keyhani et al. [3], and Subramaniam et al. [4] built physically correct numerical models of the nasal cavity. They did a numerical analysis with laminar and stationary flows. Airflow patterns on both sides were not compared. Wang et al. [5] limited their study with only one nasal cavity. Wen et al. [6] discussed flow pattern in the turbinate and nasal valve. Kai Zhao et al. [7] analyzed the process of mass transport in nasal cavity.

In this study, velocity profiles, iteration plots, pressure distribution, streamline and pathline patterns for two dimensional airflows inside both sides of the human nasal cavity of healthy and also infected persons are analyzed to compute the velocity and pressure at different points of the nasal cavity particularly in the olfactory region. This analysis helps to understand and visualize the implications for olfaction. Velocity is prescribed as the inlet condition. The advantage of this method is that velocity, pressure, and density are closely related. Therefore the end results in terms of velocity can be easily converted to density and pressure using Navier Stokes equations.

The remainder of this paper is organized as follows. Section II presents mathematical modeling, governing differential equations, assumptions and boundary conditions. Section III exposes the methodology in detail. Section IV reports our relevant discussion. Concluding remarks are given in Section V.

M.V.Shyla is with the Department of Mathematics, Sathyabama University, Chennai-600119, Tamilnadu (Phone: +919962737191, e-mail: shylamv@yahoo.com).

Dr. K. B. Naidu, Professor, is with the Department of Mathematics, Sathyabama University, Chennai-600119, Tamilnadu. (Phone: +919789068471, e-mail: kbnaidu999@gmail.com).

II. Mathematical Modeling

Laminar flow is assumed. Solid particles represent a negligible mass fraction and hence ignored. Body forces are all neglected. Steady flow is considered. A simple model of basic sniffing process is taken for this study. The sniffer approaches the vapor cloud of air of volume V inhaling a volume V_1 thro' the nostril over time interval Δt. This air is transferred by the nose from V to its internal sensor chamber with volume V_2, at a flow rate $Q= V_1/\Delta t$.

A. Governing Differential Equation

Navier Stokes system of equations for a two dimensional, viscous, incompressible flow

$$\nabla.\bar{q} = 0$$

$$\rho\left(\frac{\partial\vec{q}}{\partial t} + \vec{q}.\nabla\vec{q}\right) = -\nabla p + \mu\nabla^2\vec{q} \quad (1)$$

$\vec{q} = u\vec{\imath} + v\vec{\jmath}$ is the velocity vector where u and v are the velocity components in the x & y directions respectively, p is pressure, ρ is density, and μ is viscosity.

In nondimensional form, we have

$$\left(\frac{\partial\vec{q}}{\partial t} + \vec{q}.\nabla\vec{q}\right) = -\nabla p + \frac{1}{Re_L}\nabla^2\vec{q} \quad (2)$$

In expanded 2D cartesian coordinates, the equations are

$$\frac{\partial u}{\partial x} + \frac{\partial v}{\partial y} = 0$$

$$\left(\frac{\partial u}{\partial t} + u\frac{\partial u}{\partial x} + v\frac{\partial u}{\partial y}\right) = -\frac{\partial p}{\partial x} + \frac{1}{Re_L}\left(\frac{\partial^2 u}{\partial x^2} + \frac{\partial^2 u}{\partial y^2}\right)$$

$$\left(\frac{\partial v}{\partial t} + u\frac{\partial v}{\partial x} + v\frac{\partial v}{\partial y}\right) = -\frac{\partial p}{\partial y} + \frac{1}{Re_L}\left(\frac{\partial^2 v}{\partial x^2} + \frac{\partial^2 v}{\partial y^2}\right) \quad (3)$$

In compact Vector form,

$$\frac{\partial\vec{Q}}{\partial t} + \frac{\partial\vec{E_i}}{\partial x} + \frac{\partial\vec{H_i}}{\partial y} = \frac{\partial\vec{E_v}}{\partial x} + \frac{\partial\vec{H_v}}{\partial y}$$

where

$$\overrightarrow{Q} = \begin{bmatrix} 0 \\ u \\ v \end{bmatrix} ; \overrightarrow{E_\iota} = \begin{bmatrix} u \\ u^2 + p \\ uv \end{bmatrix} ; \overrightarrow{H_\iota} = \begin{bmatrix} v \\ vu \\ v^2 + p \end{bmatrix} ;$$

$$\overrightarrow{E_v} = \begin{bmatrix} 0 \\ \tau_{xx} \\ \tau_{xy} \end{bmatrix} \quad ; \overrightarrow{H_v} = \begin{bmatrix} 0 \\ \tau_{yx} \\ \tau_{yy} \end{bmatrix}$$

$$\tau_{xx} = \frac{2}{Re_L}\frac{\partial u}{\partial x} \quad \tau_{yy} = \frac{2}{Re_L}\frac{\partial v}{\partial y}$$

$$\tau_{xy} = \frac{1}{Re_L}\left(\frac{\partial u}{\partial y} + \frac{\partial v}{\partial x}\right) = \tau_{yx} \tag{4}$$

$\overrightarrow{Q}$ is the vector containing the primitive variables. $\overrightarrow{E_\iota}$ & $\overrightarrow{H_\iota}$ are the vectors containing the inviscid fluxes in the x and y directions. $\overrightarrow{E_v}$ & $\overrightarrow{H_v}$ are the vectors containing the viscous fluxes in the x & y directions respectively.

Transformation of the governing equations in physical space with cartesian coordinates (x,y,t) to computational space with generalized curvilinear coordinates (ξ, η, τ) by using the following transformations

$$\tau = \tau(t) = t;\ \xi = \xi(x, y, t);\ \eta = \eta(x, y, t) \tag{5}$$

By applying chain rule,

$$\begin{pmatrix} d\tau \\ d\xi \\ d\eta \end{pmatrix} = \begin{pmatrix} 1 & 0 & 0 \\ \xi_t & \xi_x & \xi_y \\ \eta_t & \eta_x & \eta_y \end{pmatrix} \begin{pmatrix} dt \\ dx \\ dy \end{pmatrix} \tag{6}$$

The inverse transformations are given by

$$t = t(\tau) = \tau; x = x(\tau, \xi, \eta); y = y(\tau, \xi, \eta) \tag{7}$$

By applying chain rule,

$$\begin{pmatrix} dt \\ dx \\ dy \end{pmatrix} = \begin{pmatrix} 1 & 0 & 0 \\ x_\tau & x_\xi & x_\eta \\ y_\tau & y_\xi & y_\eta \end{pmatrix} \begin{pmatrix} d\tau \\ d\xi \\ d\eta \end{pmatrix}$$

Hence

$$\begin{pmatrix} d\tau \\ d\xi \\ d\eta \end{pmatrix} = \begin{pmatrix} 1 & 0 & 0 \\ x_\tau & x_\xi & x_\eta \\ y_\tau & y_\xi & y_\eta \end{pmatrix}^{-1} \begin{pmatrix} dt \\ dx \\ dy \end{pmatrix} \quad \begin{pmatrix} 1 & 0 & 0 \\ \xi_t & \xi_x & \xi_y \\ \eta_t & \eta_x & \eta_y \end{pmatrix} = \begin{pmatrix} 1 & 0 & 0 \\ x_\tau & x_\xi & x_\eta \\ y_\tau & y_\xi & y_\eta \end{pmatrix}^{-1} \tag{8}$$

This yields the following metric relationships

$$\xi_x = Jy_\eta;\ \xi_y = -Jx_\eta;\ \eta_x = -Jy_\xi;\ \eta_y = Jx_\xi$$

$$\xi_t = J(x_\eta y_\tau - x_\tau y_\eta);\ \eta_t = J(x_\tau y_\xi - x_\xi y_\tau) \tag{9}$$

J is the determinant of the Jacobian matrix of the transformation defined by

$$J = \left|\frac{\partial((\xi,\eta)}{\partial(x,y)}\right| \text{ or } J = \frac{1}{(x_\xi y_\eta - x_\eta y_\xi)} \tag{10}$$

In computational space, the governing differential equations in compact form become

$$\frac{\partial \hat{Q}}{\partial \tau} + \frac{\partial \widehat{E_\iota}}{\partial \xi} + \frac{\partial \widehat{H_\iota}}{\partial \eta} = \frac{\partial \widehat{E_v}}{\partial \xi} + \frac{\partial \widehat{H_v}}{\partial \eta}$$

where $\hat{Q} = \frac{\vec{Q}}{J}$

$$\widehat{E_\iota} = \frac{1}{J}\left(\xi_t \vec{Q} + \xi_x \overrightarrow{E_\iota} + \xi_y \overrightarrow{H_\iota}\right)$$
$$\widehat{H_\iota} = \frac{1}{J}\left(\eta_t \vec{Q} + \eta_x \overrightarrow{E_\iota} + \eta_y \overrightarrow{H_\iota}\right)$$
$$\widehat{E_v} = \frac{1}{J}\left(\xi_x \overrightarrow{E_v} + \xi_y \overrightarrow{H_v}\right)$$
$$\widehat{H_v} = \frac{1}{J}\left(\eta_x \overrightarrow{E_v} + \eta_y \overrightarrow{H_v}\right) \tag{11}$$

$\widehat{(Q)}$ is the vector containing the primitive variables. $\widehat{E_\iota}$ & $\widehat{H_\iota}$ are the vectors containing the inviscid fluxes in the ξ and η directions. $\widehat{E_v}$& $\widehat{H_v}$ are the vectors containing the viscous fluxes in the ξ & η directions respectively.

$$\widehat{Q} = \frac{1}{J}\begin{bmatrix} 0 \\ u \\ v \end{bmatrix} ; \widehat{E_\iota} = \frac{1}{J}\begin{bmatrix} U \\ uU + p\xi_x \\ vU + p\xi_y \end{bmatrix} ; \widehat{H_\iota} = \begin{bmatrix} V \\ uV + p\eta_x \\ vV + p\eta_y \end{bmatrix} ;$$

$$U = u\xi_x + v\xi_y; V = u\eta_x + v\eta_y$$

$$\widehat{E_v} = \frac{1}{JRe_L}\begin{bmatrix} 0 \\ (\nabla\xi.\nabla\xi)\mathrm{u}_\xi + (\nabla\xi.\nabla\eta)\mathrm{u}_\eta \\ (\nabla\xi.\nabla\xi)\mathrm{v}_\xi + (\nabla\xi.\nabla\eta)\mathrm{v}_\eta \end{bmatrix};$$

$$\widehat{H_v} = \frac{1}{JRe_L}\begin{bmatrix} 0 \\ (\nabla\eta.\nabla\xi)\mathrm{u}_\xi + (\nabla\eta.\nabla\eta)\mathrm{u}_\eta \\ (\nabla\eta.\nabla\xi)\mathrm{v}_\xi + (\nabla\eta.\nabla\eta)\mathrm{v}_\eta \end{bmatrix}$$

$$\tau_{xx} = \frac{2}{Re_L}\left(\xi_x u_\xi + \eta_x u_\eta\right);\ \tau_{yy} = \frac{2}{Re_L}\left(\xi_y v_\xi + \eta_y v_\eta\right);$$

$$\tau_{xy} = \frac{1}{Re_L}\left(\xi_y u_\xi + \eta_y u_\eta + \xi_x v_\xi + \eta_x v_\eta\right);\ \tau_{xy} = \tau_{yx} \tag{12}$$

For a steady state: $\frac{\partial \vec{Q}}{\partial t} = 0;\ \frac{\partial \hat{Q}}{\partial \tau} = 0; x_\tau = 0; y_\tau = 0;$
$\xi_t = 0; \eta_t = 0$

Hence the equation reduces to the form:

$$\frac{\partial \widehat{E_\iota}}{\partial \xi} + \frac{\partial \widehat{H_\iota}}{\partial \eta} = \frac{\partial \widehat{E_v}}{\partial \xi} + \frac{\partial \widehat{H_v}}{\partial \eta} \tag{13}$$

A distorted region in physical space is mapped into a rectangular region in the computational space. The governing equations are solved in the computational space to obtain the unknown flow field variables u, v, & p. The computed information is then transferred back to the physical space [8], [9].

B. Boundary Conditions

A two dimensional, laminar, incompressible, steady airflows inside the human nasal cavity of healthy and also infected persons are considered. *A* velocity of 0.2 m/s is applied at the inlet (inferior meatus). The walls of the nasal cavity are assumed to be rigid. No slip boundary condition on the velocity is considered at the mucous air interphase. The operating air pressure is kept at 101325 Pascal (Pa) at both nostrils with $\rho = 1.225$ kg/m^3 and $\mu = 1.7894$e-05 kg/m-s.

III. Methodology

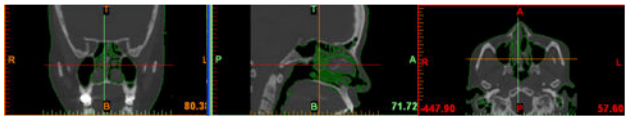

(a) (b) (c)

Fig. 1 CT image generated by MIMICS (a) Coronal view (b)Axial view (c) Sagittal view

Computer simulation is used in this study to analyze the two dimensional airflow patterns in the human nasal cavity to visualize implications for olfaction. The CT scans of 6 healthy persons and 2 other persons infected by nasal congestion and inflammation were considered for study. The CT images of the subjects were loaded in MIMICS 10 software. MIMICS display all images in three different views namely the coronal view (xz-view), axial view (xy-view), and sagittal view (yz-view) as shown in Fig. 1. The coronal view best illustrates the nasal structure. Different segmentation techniques like threshold, region growing, and crop masking are applied. A three dimensional surface is quickly generated by Mimics. The nasal geometry taken from mimics is fed into Gambit software using which a computational volume is created in which mesh is generated. The number of nodes and quadrilateral cells for different subjects under consideration are given in Table I. The mesh from Gambit software is then exported to Fluent 6.3 software where a 2D analysis is done. A finite volume scheme is employed by the software. The governing differential equations namely the continuity equation and Navier-Stokes equations in the integral form for the entire domain under consideration is discretized into each element at the outset. Implicit second order scheme is employed. All the elements are later assembled resulting in a large linearized matrix. It is solved iteratively by a segregated solver. The solution to the system of equations which govern the process is generated iteratively. The solution provides a clear and detailed information of velocity, pressure, pathline and streamline pattern. Initially, default values are used and then slightly modified for best convergence rate.

TABLE I
GRID DATA FOR LEFT AND RIGHT NASAL CAVITY

Persons	Left		Right	
	No. of Nodes	No. of quadrilateral cells	No. of Nodes	No. of quadrilateral cells
1.	12187	11442	10051	9334
2.	11,059	10478	10141	9575
3.	12292	11446	11935	11242
4.	12674	12149	10678	10221
5.	14571	13976	13952	13420
6.	13065	12484	9964	9444
7.	11312	10618	13465	12604
8.	8272	7917	10887	10402

IV. Analysis of Results and Discussion

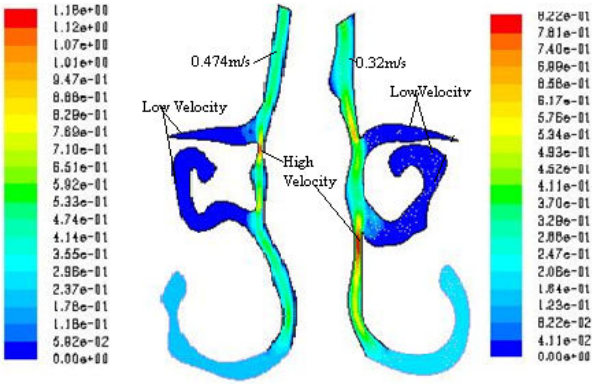

Fig. 2 Velocity profile of a healthy person 1

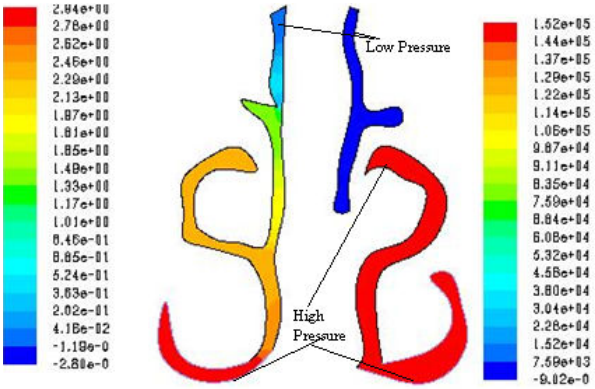

Fig. 3 Pressure distribution of an infected person 7

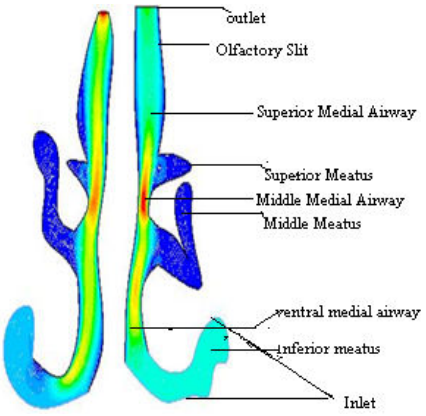

Fig. 4 Streamline pattern of person 5

Fig. 5 Pathline pattern of person 1

The geometry of the nasal cavity and the flow rate are the factors that contribute to the airflow patterns. For a physically normal human nasal cavity, the left and the right sides differ in geometry and morphological differences can be found between individuals [6]. Numerical studies reveal that highest velocities of flow appear in the middle of airway and low flows in nasal meatuses. Only part of the inspired air flows through the nasal cavity and reaches the olfactory region [7], [10] as shown in Fig. 2. It also gives the velocity at different points of the nasal cavity. Different values are represented by different colours with the lowest value represented by blue and highest value represented by red. Detailed description of velocity at olfactory region for different patient is given in Table II. The velocity values indicate normal air flow in healthy patients. But very low velocity is observed in the nasal cavity of infected patient when compared to healthy nassal cavity without any abnormalities. Pressure variations are tabulated in Table II. From Fig. 3, pressure distribution at different points of left and right nasal cavities can be viewed. High pressure at the inlet and negative pressure is observed in the olfactory region of infected person which is an indication of obstruction of air flow which is clearly illustrated in Fig. 3. Pressure is normal in the case of healthy persons. Deviation in the results is due to the different geometry, abnormalities, or infections in the nasal cavity. The convergence of the results correct to 3 decimal places is checked as depicted in iteration plots in Fig. 6. It also demonstrates the solution of continuity and Navier Stokes equation at every time step for 100 iterations. The path followed by the fluid particles can be viewed from the graph of pathlines in Fig. 5. The streamline pattern in Fig. 4 clearly shows airflow through the nasal cavity to the olfactory slit in the direction of velocity and hence the implication for olfaction.

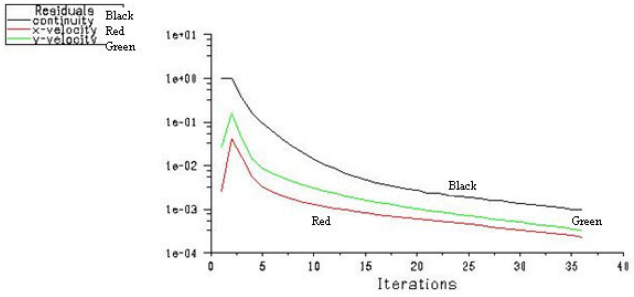

Fig. 6 Velocity iteration plot to check convergence

TABLE II
VELOCITY AND PRESSURE DATA FOR LEFT AND RIGHT NASAL CAVITY

Person	Left		Right	
	Velocity in (m/s) Olfactory slit	Pressure in(Pa) Olfactory slit	Velocity in (m/s) Olfactory slit	Pressure in pascal(Pa) Olfactory slit
1.	0.32	0.09	0.474	0.112
2.	0.14	0.0144	0.345	0.0311
3.	0.839	-9.67	0.0613	0.0525
4.	0.99	2.14	1.49	0.643
5.	0.317	0.017	0.469	0.68
6.	0.376	0.00678	0.364	0.228
7.	0.0775	-0.00902	0.656	0.00416
8.	0.0758	-0.00189	0.0385	-0.00407

V. CONCLUSION

Thus this study has clearly depicted the fact that only part of the inspired air reaches the olfactory region. The nasal cavity structure contributes to this factor, thereby protects the human health from the risk of inhaled materials to a great extent. Changes in the anatomy of the nasal cavity leads to great changes in the airflow pattern which is clearly depicted by the variation of the velocity and pressure at various points of the nasal cavity for different patients. Infections and abnormalities in the nasal cavity affect the sniffing process. This analysis can serve as a powerful tool in preparation of preoperative nasal surgery. Numerical simulation of airflow helps us to visualize implications for olfaction. The significance of this study is to simply observe and analyze the airflow through human nasal cavity for designing artificial sensors used for trace detection to defend bioterrorism.

REFERENCES

[1] Gary S. Settles, "Sniffers: Fluid-Dynamic Sampling for Olfactory Trace Detection in Nature and Homeland Security"- The 2004 Freeman Scholar Lecture.
[2] Elad D, Liebental R, Wening B L, Einav S. Analysis of air flow patterns in the human nose. Med and Biol Eng and Comput 1993; 31:585- 592.
[3] Keyhani K., Scherer P.W. and Mozell M.M., Numerical Simulation of Airflow in the Human Nasal Cavity, *J. Biomech Eng.*, 117, 1995, 429-441.
[4] Subramaniam R.P., Richardson R.B., Morgan K.T., Kimbell J.S. and Guilmette R.A., Computational Fluid Dynamics Simulations of Inspiratory Airflow in the Human Nose and Nasopharynx, *Inhal. Toxicol.*, **10**,1998,91–120.
[5] Wang K., Jr.T.S.D., Morrison E.E., Vodyanoy V.J., *Numerical Simulation of Air Flow in the Human Nasal Cavity*, Proceeding of the 2005 IEEE, 2005,5607-5610.
[6] J.Wen 1, K.Inthavong1, Z.F.Tian1, J.Y.Tu1, C.L.Xue2 and C.G.Li2 Airflow Patterns in Both Sides of a Realistic Human Nasal Cavity for Laminar and Turbulent Conditions, "16th Australian Fluid Mechanics Conference, Crown Plaza, Gold Coast, Australia, 2-7 December 2007, pp. 68-74.
[7] Zhao K, Scherer PW, Hajiloo SA, Dalton P. Effect of anatomy on human nasal airflow and odorant transport patterns. Chem Senses 2004; 29(5): 365-379.
[8] John F. Wendt Editor, Computational Fluid Dynamics An Introduction, with contributions by John D. Anderson Jr., Joris Degroote, Gerard Degrez, Erik Dick, Roger Grundmann and Jan Vierendeels, Third Edition. ISBN: 978-3-540-85055-7.
[9] Joel Guerrero, Numerical Simulation of the unsteady Aerodynamics of flapping flight, Thesis chapter 3, pp, 34-51.
[10] Kelly J.T., Prasad A.k., and Wexler A.S., Detailed Flow Patterns in the Nasal Cavity, *J Appl. Physiol.*, 89, 2000,323-337.